49th AIAA Aerospace Sciences Meeting including the New Horizons Forum and Aerospace Exposition
4 - 7 January 2011, Orlando, Florida

AIAA 2011-642

# Preliminary Aerodynamic Shape Optimization Of A Blended-Wing-Body Aircraft Configuration

Nimeesha B. Kuntawala[*], Jason E. Hicken[†] and David W. Zingg[‡]

*Institute for Aerospace Studies, University of Toronto, Toronto, Ontario, M9N 3Z4, Canada*

**The preliminary results of the flow analysis and aerodynamic shape optimization of a 2-crew, 10-passenger blended-wing-body aircraft configuration are presented. Flow analysis is performed using an Euler-based parallel Newton-Krylov-Schur flow solver. A sequential quadratic programming algorithm that allows for linear and nonlinear constraints is employed for the optimization. Gradients are efficiently computed through the discrete adjoint approach. Results of two independent, single-point planform optimizations to minimize the sum of induced and wave drag at transonic speed are presented and compared. For a blended-wing-body aircraft cruising at Mach 0.85, a reduction in induced and wave drag of almost 40%, relative to the baseline geometry, is achieved at the target lift coefficient. A partial section optimization results in more than 50% drag reduction relative to the baseline geometry.**

## Nomenclature

| | |
|---|---|
| $\alpha$ | Angle of attack, degrees |
| $C_L$ | Lift coefficient |
| $C_D$ | Drag coefficient |
| $C_p$ | Pressure coefficient |
| $x/c$ | $x$-coordinates non-dimensionalized by root-chord length |
| $y/c$ | $y$-coordinates non-dimensionalized by root-chord length |
| $MTOW$ | Maximum Take-Off Weight |

## I. Introduction

Increasing environmental concerns and fuel prices drive the need for a more fuel efficient means of air travel. The blended-wing-body (BWB) configuration is one such promising alternative. Liebeck[1] showed that a BWB designed for approximately 800 passengers and a range of 7000 nautical miles results in a 27% reduction in fuel consumption per passenger-km compared to a conventional aircraft configuration.

Several features of the BWB configuration make it advantageous to the tube-and-wing configuration. From an aerodynamics perspective, one such aspect is the lift-generating centerbody of the BWB — a gain over the cylindrical fuselage of a conventional aircraft.[2] The BWB shape has also been shown to be more naturally area-ruled, making higher cruise Mach numbers more attainable with a lower drag penalty.[1,3] From a noise-reduction perspective, since the BWB eliminates the tail, has smooth lifting surfaces, and minimizes exposed edges and cavities, it is inherently a low-noise design.[4] From a structural perspective, the lift and payload are much more in line with each other on the BWB than on a conventional aircraft.[1]

Despite the promise of the BWB, certain challenges exist. One such challenge is posed by the BWB's non-cylindrical pressure vessel, which results in increased structural weight in order to handle the increased stresses.[5] With the elimination of the tail, control and stability also become issues for this configuration.

---

[*] Masters Candidate, nimeesha@oddjob.utias.utoronto.ca, AIAA Student Member

[†] Postdoctoral Fellow (currently a Postdoctoral Fellow at Stanford University), jehicken@stanford.edu, Member AIAA

[‡] Professor and Director, Tier 1 Canada Research Chair in Computational Aerodynamics, J. Armand Bombardier Foundation Chair in Aerospace Flight, dwz@oddjob.utias.utoronto.ca, Associate Fellow AIAA

The BWB configuration is essentially a flying wing which must carry a payload with minimum structural weight penalty and generate lift with minimum drag penalty, while operating in a stable manner over its full flight envelope. This makes for a highly integrated aircraft configuration which ultimately requires significant research employing a multidisciplinary perspective.[6]

Various research groups, including Liebeck *et al.*,[1,7–9] have studied the BWB configuration from both an aerodynamics and multidisciplinary perspective. At Cranfield, as part of the European Multidisciplinary Optimization of a Blended-Wing-Body project, Qin *et al.* have also carried out various optimizations using a high-fidelity Reynolds-averaged Navier Stokes solver and have considered interesting situations such as a BWB with forward sweep on the outer wing.[2,10,11] At Cambridge and MIT, the Silent Aircraft Initiative considered a BWB-type aircraft with a focus on reducing noise, such that the aircraft is inaudible outside the airport boundary.[4] Pambagjo *et al.*[12,13] have studied the BWB concept applied to medium-sized aircraft. Peigin and Epstein[14] also performed a high-fidelity CFD-driven optimization on the BWB configuration, performing both single-point and multi-point optimizations. Other interesting concepts include a hydrogen fuel cell powered BWB evaluated by NASA[15] and C-wing BWBs.[16]

Our project consists of three steps:

- inviscid aerodynamic shape optimization (ASO) with a focus on cruise conditions;
- Reynolds-averaged Navier-Stokes ASO incorporating additional low-speed requirements;
- multi-disciplinary optimization (MDO).

By initially focusing on aerodynamics, our objective is to identify the optimal aerodynamic shape in the absence of multi-disciplinary considerations as a preliminary step to explore the design space and attempt to find significant drag reductions. This aerodynamically optimized geometry might then serve as a starting point for a multi-disciplinary optimization taking into consideration structural and handling factors.

For the first step in this process, we explore the design space with a fixed-section, planform optimization. The next step involves freeing up the airfoil sections for section optimization. These single-point optimizations will be followed by multipoint optimizations over an expected range of operating conditions.

In this paper, we describe the preliminary results of aerodynamic shape optimization of BWB configurations based on the Euler equations to reduce induced and wave drag contributions. We present a brief description of the design mission considered, our sizing methodology for the BWB, baseline geometry parameterization, an aerodynamic analysis of a baseline configuration, and finally, optimization results. In particular, results for fixed section, planform optimizations are presented, followed by preliminary results for section optimization.

## II. Design Mission

Table 1 summarizes the design mission requirements for the BWB studied in this paper. These specifications drive the internal volume constraints as defined in the following section, which in turn influence the BWB planform area sizing and weight estimation described in Section IV.

| | |
|---|---|
| **Capacity** | |
| Crew | 2 |
| Passengers | 10 |
| **Performance Parameters** | |
| Cruise Mach | 0.85 |
| Range (NM) | 6000 |
| Cruise Altitude (ft) | 41,000 |

**Table 1. Design mission specifications for baseline BWB.**

| Fuselage Parameters | |
|---|---|
| Seat pitch (inches) | 35 |
| Abreast | 2/4 |
| Height of pressurized cabin (ft) | 7.17 |

Table 2. User-speciþed requirements for baseline BWB geometry internal volume constraints.

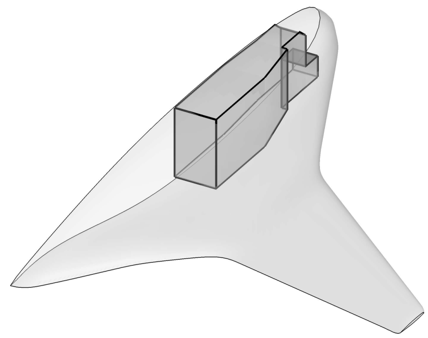

Figure 1. Half of the baseline BWB geometry with internal volume constraints.

## III. Internal Volume Constraints

SuŽcient space for crew, passengers, luggage, lavatories, and galleys is determined using a sizing tool based on Refs. 17 and 18. For user-speciþed parameters, such as number of passengers, seat pitch, height of the cabin, etc., a polyhedron representing the minimum external bounds of the interior layout is generated. Based on the results, minimum chord length constraint values and spanwise positions of these constraints can be determined for the optimization process. Figure 1 shows these minimum external bounds for the speciþcations in Tables 1 and 2.

## IV. Weight Estimation and Planform Area Sizing

Sizing the baseline geometry is not limited to ensuring that the outer BWB shell envelops the polyhedron representing minimum external bounds. Two additional factors are considered: weight estimation and planform area sizing, in order to ensure a reasonable wing loading relative to an existing, comparable tube-and-wing aircraft. As a rough rule of thumb, based on data provided by Liebeck,[1] a target wing loading of approximately 70% of that for a selected tube-and-wing aircraft was set. In addition, we also required that the target $C_L$ value be within a reasonably expected range of values.

For the weight estimation, the maximum-take-oÞ-weight ($MTOW$) is sub-divided as follows:

$$MTOW = W_{\text{empty}} + W_{\text{payload}} + W_{\text{fuel}} \tag{1}$$

where $W_{\text{empty}}$ is the aircraft empty weight, $W_{\text{payload}}$ is the payload weight, and $W_{\text{fuel}}$ is the fuel weight. The assumed fuel weight is a value appropriate for the design range in Table 1.

The aircraft empty weight is further broken down as follows:

$$W_{\text{empty}} = W_{\text{fuselage}} + W_{\text{wing}} + W_{\text{þxed}} \tag{2}$$

where $W_{\text{fuselage}}$ is the fuselage weight, $W_{\text{wing}}$ is the outer wing weight, and $W_{\text{þxed}}$ is the þxed weight. The fuselage weight equation is unique for the BWB conþguration and as such, equations developed by Bradley[17] based on BWB FEM models are used. These equations are primarily for larger BWB aircraft; however, they provide suŽcient means of a rough estimation for our purposes. Furthermore, while Bradley further divides the main body of the aircraft into a pressurized fuselage and non-pressurized aft-body which supports the engines, the entire main body is treated as a pressurized fuselage for this work. As such, the aft-body equations are not employed. The wing weight is evaluated using an equation for existing aircraft presented by Torenbeek.[18] The þxed weight consists of furnishings, avionics, controls, etc. and was estimated using averaged values for existing tube-and-wing aircraft of comparable size.[19,20] These equations reduce to functions of the $MTOW$ and thus the weight can be solved for.

| Geometric Parameters | |
|---|---|
| Root-chord length (ft) | 55.7 |
| Semi-Span (ft) | 34.7 |
| Aspect Ratio | 3.17 |
| Half Planform Area (sq. ft) | 759 |
| **Performance Parameters** | |
| $C_L$ | 0.357 |
| Estimated MTOW (lb) | 89000 |

Table 3. Key geometric and performance parameters for baseline BWB geometry.

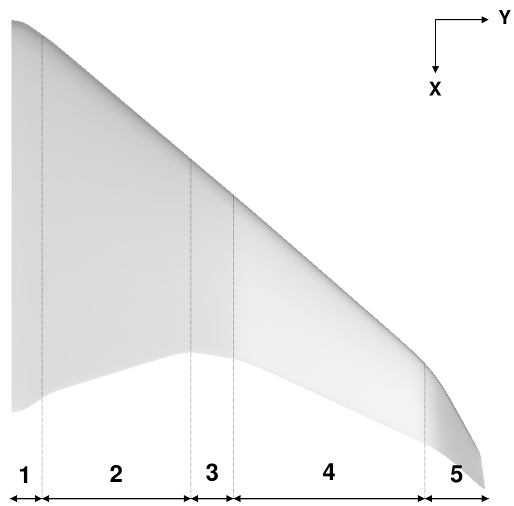


Figure 2. Blended-wing-body geometry representation.

The weight estimation is also dependent on the planform area. Given this relationship, our rough rule of the thumb for wing loading, and the target $C_L$ considerations, the planform area was manually modiþed and sized around the internal volume polyhedron. Key geometric and performance parameters resulting from this sizing are listed in Table 3.

## V. Geometry Parameterization

B-spline-based surface patches { speciþcally, employing cubic B-splines { are used to parameterize our smooth, aerodynamic geometries, such as those studied in this project. The control points of these cubic B-splines can then be used as design variables, enabling modiþcation of the aerodynamic surface.[21]

Various BWB geometries can be generated with our B-spline-based geometry parameterization. As part of this parameterization, the aircraft is deþned by þve diÞerent sections, shown in Figure 2. For each of these sections, diÞerent airfoils can be speciþed and are þt with B-spline curves. The control point coordinates from this þtting are then used to deþne the $x$- and $z$-coordinates of the control points deþning the B-spline surface patch for the baseline BWB, where the $x$-coordinates are in the chordwise direction. The $y$-coordinates, which are in the spanwise direction, are speciþed at equal intervals over the user-speciþed semi-span of the aircraft. For sections 1 to 3 in Figure 2, the sweep, chord-lengths and span can be modiþed. In addition to these parameters, twist and dihedral can also be added to sections 4 and 5, which make up the outer wing. Based on these parameters, the control point coordinate values in each direction are modiþed to generate the desired baseline shape.

In principle, it is possible to consider almost arbitrary geometries within the feasible design space deþned by the constraints. In practice, however, it is initially preferable to consider various baseline shapes with

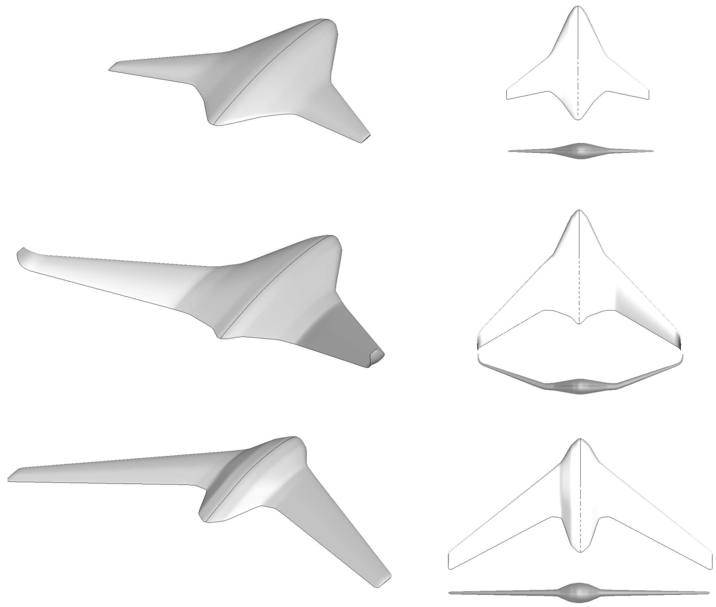

**Figure 3. Examples of baseline shapes which can be generated using our geometry parameterization.**

more limited exibility. Figure 3 shows sample baseline shapes that can be used as a basis for optimization. In this paper, we will present an optimization based on the þrst baseline geometry shown in Figure 3. As detailed in Section VIII, this baseline geometry is divided into a main body section and an outer wing section with þxed spans. Based on this deþnition, the shapes in Figure 3 diÞer from each other and this baseline in that they lie in diÞerent design spaces. For instance, additional sections would be added for non-planar elements such as those in the second geometry in Figure 3. As such, it is beneþcial to have a exible geometry parameterization tool such as the one described here. Ultimately, this reliance on the initial geometry will be eliminated.

## VI. Aerodynamic Analysis Of Baseline Geometry

The ow analysis is performed using a high-þdelity Euler-based parallel Newton-Krylov-Schur ow solver for multiblock structured meshes.[22] Using second-order accurate summation-by-parts (SBP) operators and scalar numerical dissipation, the Euler equations are discretized on each block. Simultaneous-approximation terms (SATs) are used to impose boundary conditions and couple block interfaces. Advantages of using SATs with SBPs include time-stability, minimum requirement of $C^0$ mesh continuity at block interfaces, accommodation of arbitrary block topologies and low interblock communication overhead.

A parallel Newton-Krylov-Schur solution strategy is used to solve the discrete Euler equations. In particular, Newton's method is applied to the discrete Euler equations in two phases: an approximate-Newton phase which ensures a suitable initial iterate is found for the second phase, an inexact-Newton phase. In order to solve the systems that arise in both these phases, a Krylov solver is employed. Speciþcally, FGMRES { Flexible Generalized Minimum RESidual method { is employed along with the parallel additive-Schur preconditioner.

The baseline geometry used for this ow analysis and the subsequent optimizations is shown in Figures 1 and 4. This is a clean geometry without control surfaces or propulsion components. The present results were obtained using an 18-block mesh with 580,800 nodes and oÞ-wall, leading edge, and trailing edge spacing of 0.005. The target $C_L$ of the baseline geometry, 0.357, is obtained at an angle of attack of 2.97 degrees, resulting in a $C_D$ of 0.02720. Given this $C_L$ value and our aspect ratio, the drag value in the case of minimum induced drag and zero wave drag would be 0.01280, indicating potential for improvement on this baseline shape.

Figure 5 shows the pressure coeŽcient plots at the target $C_L$ at the speciþed spanwise locations and indicates the presence of a strong shock on the top surface, including the main body surface. The airfoil sections for this baseline geometry are also shown. From Figure 6, with a maximum Mach number of almost

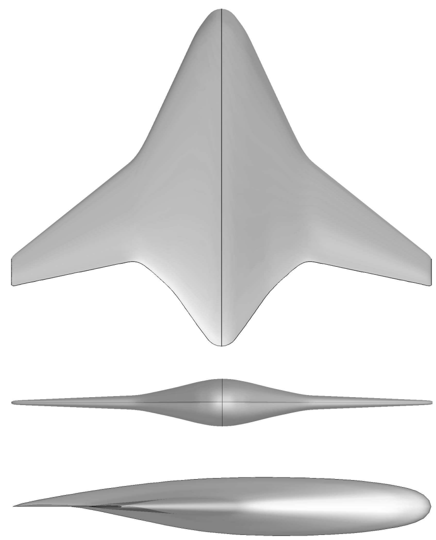

Figure 4. Baseline geometry planform, frontal and side views.

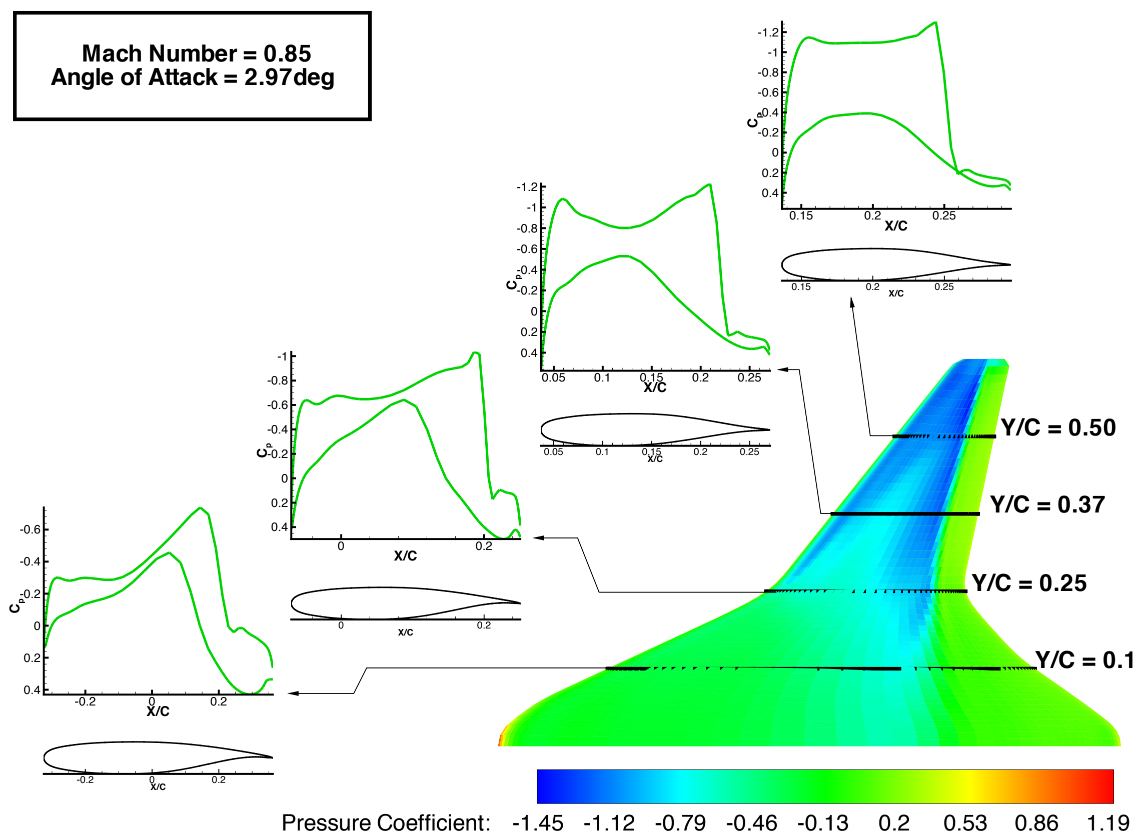


Figure 5. Pressure coeŽcient distribution over the top surface of the baseline BWB geometry and at indicated spanwise locations.

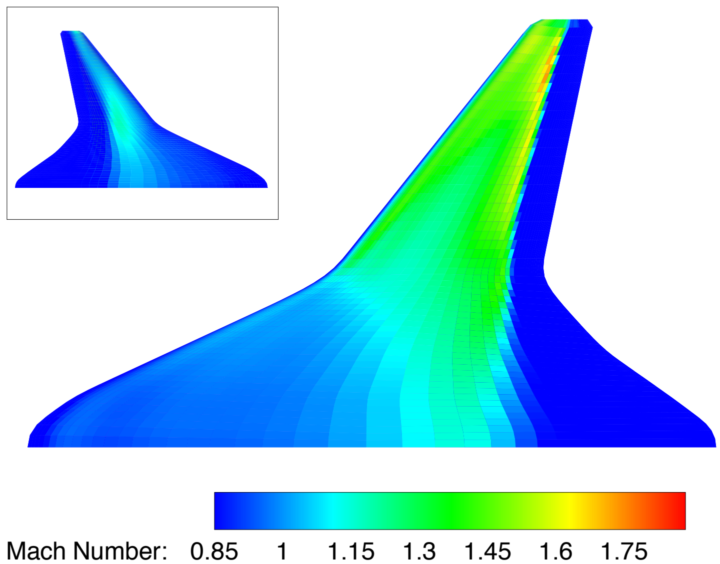


Figure 6. Mach number distribution over the top and bottom (inset) surfaces of the baseline BWB geometry.

1.89, it is evident that this shock is quite strong. These results indicate wave drag is likely a major component of the total drag, indicating further potential for improvement.

## VII. Optimization Algorithm Components

The optimization is carried out using a gradient-based algorithm,[21] which, in addition to the flow solver described in the previous section, includes the following:

**Integrated geometry parameterization and mesh movement** This parameterizes the mesh using B-spline volume control points. The geometry is parameterized as a B-spline surface, and the B-spline control points are used as design variables. For the movement of the B-spline volume control points, a linear-elasticity-based mesh movement is used. The mesh is then regenerated algebraically. The key aspect of this integrated method is the decrease in CPU time: for instance, morphing a flat plate into a BWB geometry takes 128s with the B-spline mesh movement versus 32.4h with the node-based mesh movement on a single 1500MHz Itanium 2 processor, while maintaining similar quality (orthogonality) distributions.

**Adjoint-based gradient evaluation** The cost of this method is almost independent of the number of design variables. More specifically, the discrete-adjoint approach ensures an exact gradient of the discrete objective function, further ensuring compatibility with nonlinear optimization algorithms such that the optimization process can converge fully.[23] Note that the solutions of adjoint equations for the lift constraint, as well as the mesh movement equations, are also carried out.

**Sequential quadratic programming optimization algorithm** SNOPT[24] is used to carry out the optimization and tie the above components together. Both linear and nonlinear constraints are used with this optimizer. For instance, in order to implement linear sweep, the $x$- and $y$-coordinates of leading edge control points are coupled in a linear manner. Minimum thickness constraints, on the other hand, are non-linear constraints which depend directly on the nodes. Using the chain rule, the gradients of these constraints with respect to the design variables can be obtained.

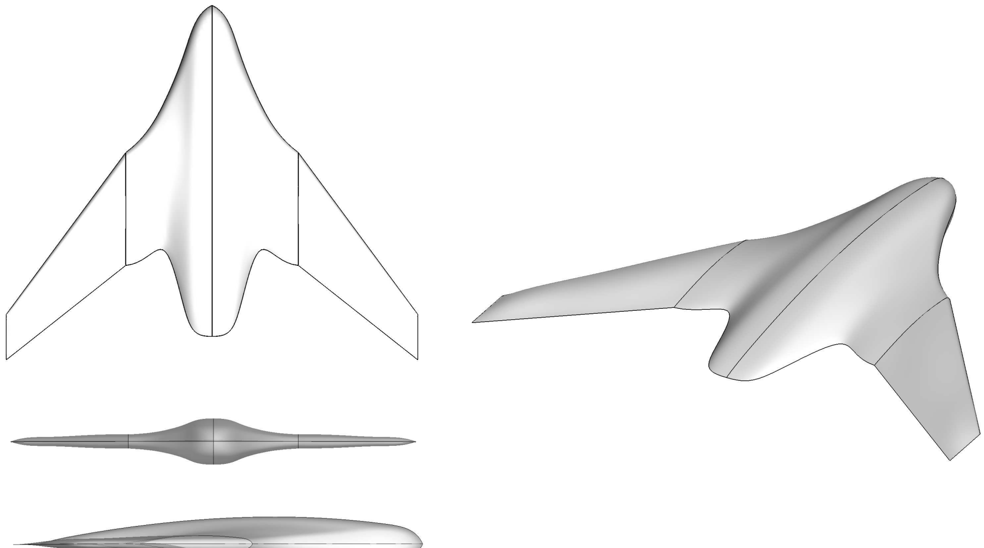

Figure 7. Various views of the optimized BWB geometry for Case A.

| Geometry | $C_D$ | Drag Reduction |
|---|---|---|
| Baseline | 0.02720 | - |
| A | 0.01837 | 32.5% |
| B | 0.01667 | 38.7% |

Table 4. Drag coefficients and percent drag reductions for baseline and optimized geometries.

# VIII. BWB with Planform Optimization

## VIII.A. Planform Optimization Problem Definition

For the optimization, the geometry is parameterized such that it consists of two sections: the main body and the outer wing. Extending this to include more sections for more complex BWB geometries (to investigate winglets, C-wing geometries, etc. for instance) would be straightforward. The airfoil sections – two modified versions of the supercritical airfoil, sc20414[25] – are maintained on the entire shape through constraints which scale the airfoils as the chord length varies. These airfoil sections are shown in Figure 5. On the main body, only the trailing edge is free to move. On the outer wing, linear sweep and twist constraints are in place. Minimum chord length constraints are applied in order to satisfy the internal volume constraints, as are spanwise width constraints. The overall span is fixed, along with the planform area. The lift coefficient is constrained at 0.357, and the objective function is the drag coefficient. Two cases are presented here and other than the following variations, the problem definitions for the two are identical:

**Case A** Fixed angle of attack of 3 degrees — since aircraft typically fly at angles of attack of 2 to 3 degrees to maintain a reasonable floor angle for passenger comfort.

**Case B** Free angle of attack with no upper or lower bounds.

## VIII.B. Planform Optimization Results

The resulting geometries are shown in Figures 7 and 8. The key differences between the two geometries include higher sweep and twist (washout) on the Case B geometry.

Table 4 compares the $C_D$ values for baseline geometry and the two optimized geometries. From this table, we can see that the Case B geometry results in lower drag by a reduction of almost 39% relative to the baseline geometry. However, this additional reduction in drag comes with an increased angle of attack of 4.43 degrees relative to Case A's 3 degrees.

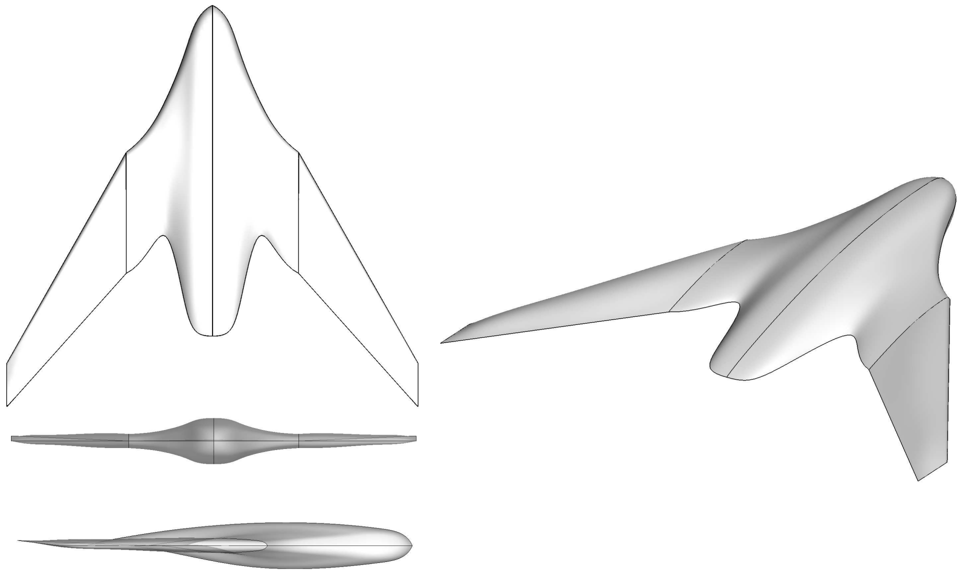

**Figure 8. Various views of the optimized BWB geometry for Case B.**

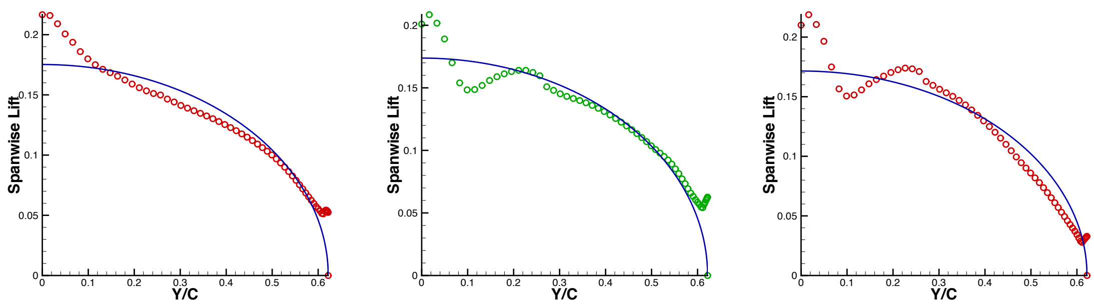


(a) Baseline geometry (b) Case A optimized geometry (c) Case B optimized geometry

**Figure 9. Spanwise load distributions**

The three sub-figures in Figure 9 show the spanwise lift distributions on the baseline and optimized geometries, compared to elliptical lift distributions. The baseline distribution is far from the elliptical lift distribution, indicating the presence of wave drag. Apart from the main body, the Case A distribution is closer to the elliptical distribution. However, the Case B distribution over the same outer wing portion appears to be tending towards a more triangular/elliptical lift distribution. The fact that this distribution on the Case B geometry leads to the lowest drag is in agreement with results found by Qin *et al.*:[2] in the case where shocks cannot be eliminated completely, an elliptical lift distribution can no longer be the goal for minimum drag design, as a compromise between wave drag due to shock wave formation at transonic speeds and induced drag due to lift is required.

Figure 10 shows pressure coefficient plots for Case B optimized geometry at the target lift coefficient of 0.357 and the same spanwise locations as on the baseline geometry (Figure 5). A shock is still present on the top surface, though not as strong as previously noted. In addition, the shock is primarily present along the outer wing leading edge. Despite the drag reduction, the maximum local Mach number on the top surface of this optimized geometry is quite high - approximately 2.44 (Figure 11). Taking a closer look at the drag polars of the baseline geometry and Case B optimized geometry (Figure 12), we see that the optimized geometry has improved performance over the range of lift coefficients shown, not just at the design point.

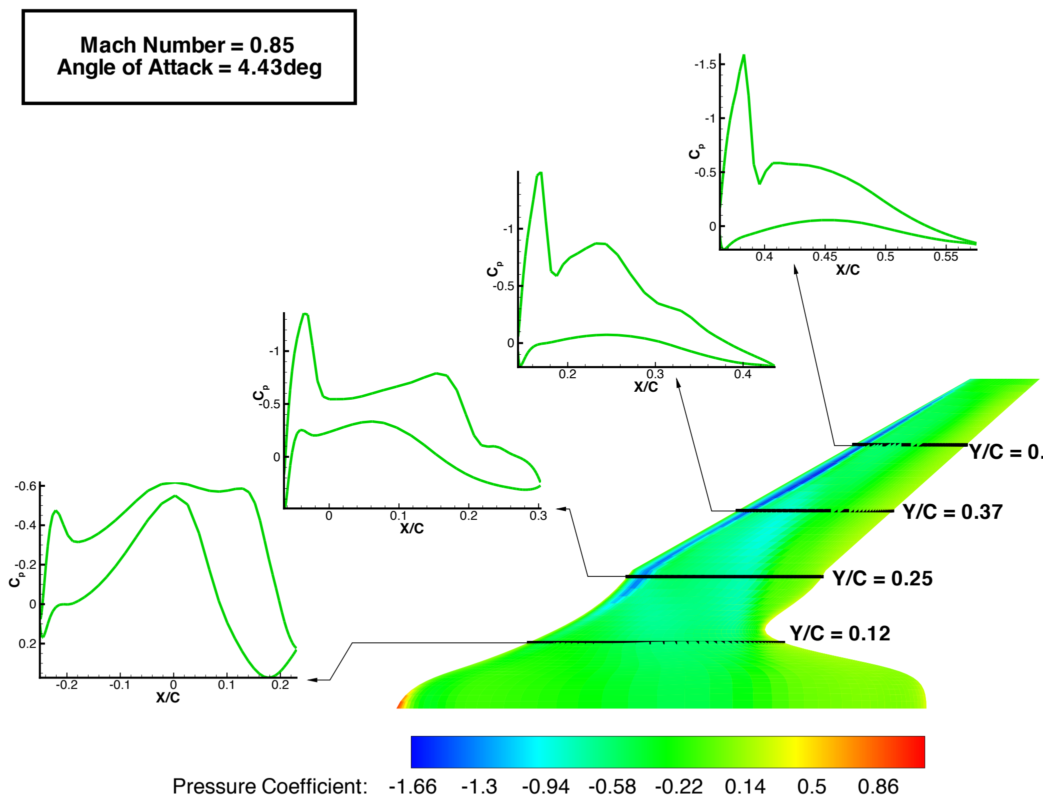


Figure 10. Pressure coefficient distribution over the top surface of the optimized BWB geometry (Case B) and at indicated spanwise locations.

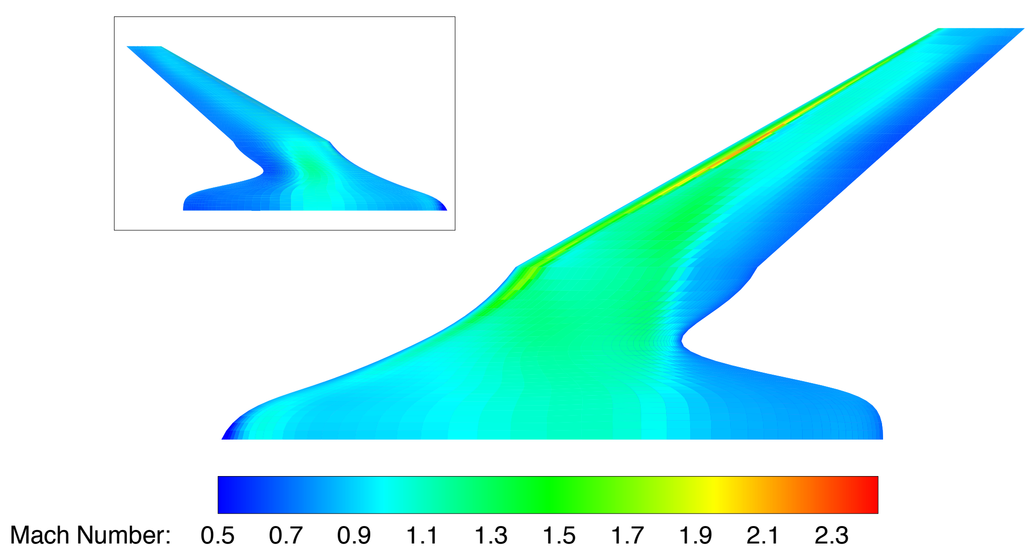


Figure 11. Mach number distribution over the top and bottom (inset) surfaces of the optimized BWB geometry (Case B).

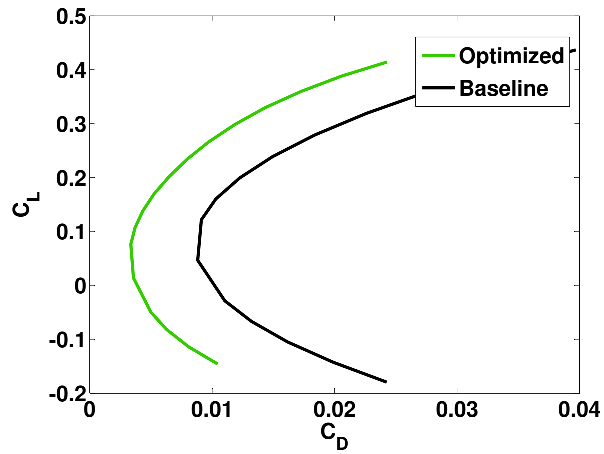


Figure 12. Comparison of the drag polars of the baseline and optimized (Case B) BWB geometries.

# IX. BWB Optimization with Increased Geometric Flexibility

## IX.A. Optimization Problem Deþnition

Similarities between this optimization and the planform optimizations include the baseline geometry and the geometry parameterization, which consists of two sections { the main body and the outer wing. In addition, the planform area is þxed. The same target $C_L$ is speciþed, and the objective function is the drag coeŽcient. The angle of attack is included as a design variable. The key diÞerences include the following: $x$- and $z$-coordinates of the control points are now design variables. Therefore, the optimizer can modify the spanwise section shapes. The span is eÞectively constrained because the $y$-coordinates are held þxed. The main body and outer wing sections of the BWB each have a speciþc volume constraint, along with constraints that prevent surfaces from crossing over each other. Collinearity constraints help ensure $C^1$ continuity at the leading edge and between the two sections. Finally, minimum thickness constraints are included to ensure the outer shell envelops the internal volume polyhedron.

## IX.B. Optimization Results

The results presented are preliminary. The optimization was feasible in the sense that all the constraints were satisþed; however, the target optimality tolerance was not achieved, i.e. the optimization did not converge fully. The resulting geometry is shown in Figure 13. The twist distribution is evident from the front and rear views of the optimized geometry. At this Mach number, one would expect a shock-free  ow. Presumably, this could be achieved by adding some sweep, but the lack of convergence of the optimizer appears to have prevented this.

| Geometry | $C_D$ | Drag Reduction |
|---|---|---|
| Baseline | 0.02720 | - |
| A (Planform) | 0.01837 | 32.5% |
| B (Planform) | 0.01667 | 38.7% |
| Section | 0.01313 | 51.7% |

Table 5. Drag coeŽcients and percent drag reductions for baseline and optimized geometries.

Table 5 compares the $C_D$ values for baseline geometry, the two planform optimization geometries and the section optimization geometry. The section optimization geometry has the most signiþcant drag reduction. At one degree, the angle of attack for this geometry is also the lowest of all shapes considered, including the baseline geometry.

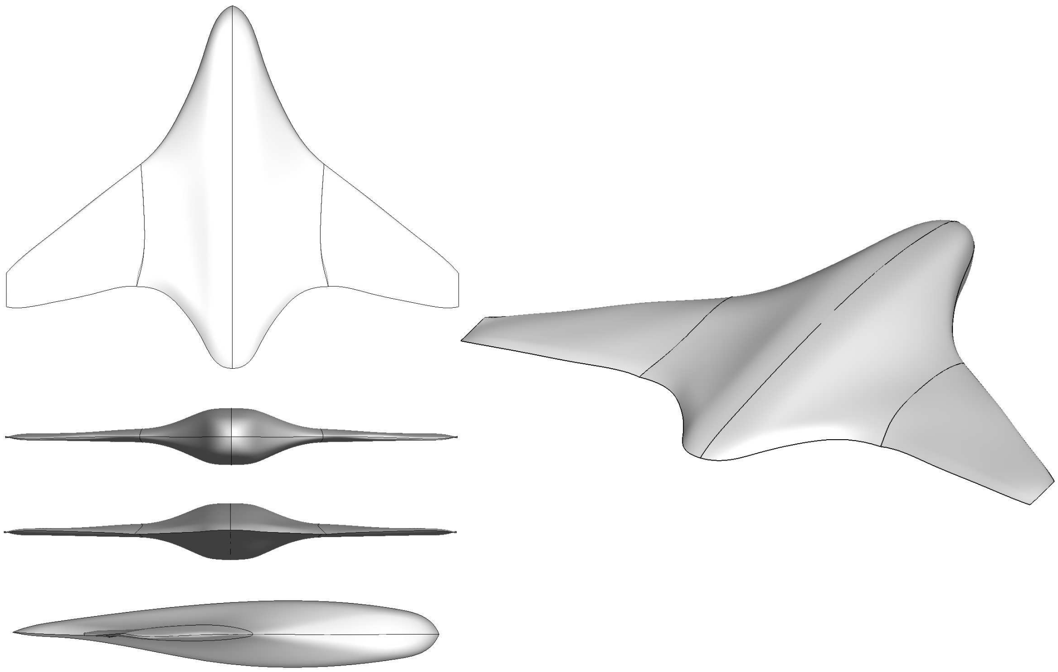

Figure 13. Various views of the section optimized BWB geometry.

Figure 14 shows pressure coefficient plots for the section optimized geometry at the target lift coefficient of 0.357 and the same spanwise locations as on the baseline geometry (Figure 5). Profiles of the optimized airfoils at these spanwise locations are also included. Despite the significant drag reduction and varying sections of this optimization, a very weak shock still exists towards the rear portion of the wing.

Figure 16 shows the spanwise lift distributions on the optimized geometry and the baseline geometry, compared to elliptical lift distributions. From this, we can see that the distribution of the section optimized geometry is much closer to the elliptical distribution than any of the shapes considered. This occurs because wave drag has been largely eliminated. It is not clear, however, how these sections would perform in a turbulent flow.

## X. Conclusions

Through a high-fidelity, inviscid Euler-based, single-point planform optimization of a 10-seater blended-wing-body aircraft configuration, almost 40% drag reduction relative to the baseline geometry has been achieved at the target lift coefficient. The potential for further drag reduction with increased geometric flexibility is demonstrated via the preliminary results for the section optimization, through which up to 52% drag reduction is achieved relative to the baseline geometry. Optimizer convergence difficulties encountered highlight the need for improvements to the optimization algorithm and the problem formulation.

## XI. Future Work

- Reformulate optimization problem to obtain full convergence;
- Multi-point optimization which ensures optimal performance over the full operating envelope;
- Consideration of non-planar geometries;
- Repetition of these studies on more refined meshes; and,
- Incorporation of structural and handling constraints.

Ultimately, similar steps will be carried out based on the solution of the Reynolds-averaged Navier-Stokes equations.

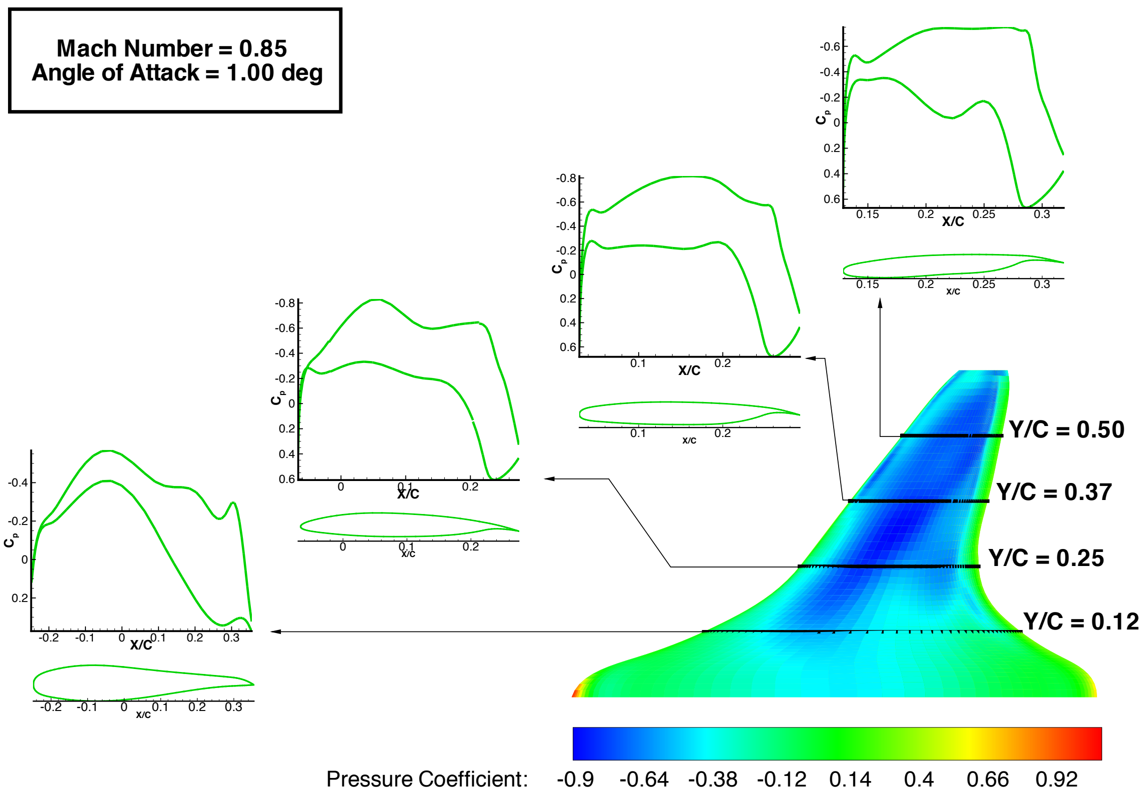


**Figure 14. Pressure coeŽcient distribution over the top surface of the section optimized BWB geometry and at indicated spanwise locations.**

## Acknowledgments

The þrst author would like to thank L. and M. Osusky for their help, as well as the Ontario Graduate Scholarship Program and the University of Toronto for þnancial support.

Computations were performed at the SciNet HPC Consortium. SciNet is funded by: the Canada Foundation for Innovation under the auspices of Compute Canada; the Government of Ontario; Ontario Research Fund - Research Excellence; and the University of Toronto.

## References

[1] Liebeck, R. H., \Design of the Blended Wing Body Subsonic Transport," *Journal of Aircraft*, Vol. 41(1), 2004, pp. 10{25.

[2] Qin, N., Vavalle, A., LeMoigne, A., Laban, M., Hackett, K., and Weinerfelt, P., \Aerodynamic Considerations of Blended Wing Body Aircraft," *Progress in Aerospace Sciences*, Vol. 40, 2004, pp. 321{343.

[3] Roman, D., Gilmore, R., and Wakayama, S., \Aerodynamics of High-Subsonic Blended-Wing-Body Conþgurations," *41st Aerospace Sciences Meeting and Exhibit, Reno, Nevada, United States*, January 2003.

[4] Diedrich, A., Hileman, J., Tan, D., Willcox, K., and Spakovszky, Z., \Multidisciplinary Design and Optimization of the Silent Aircraft," *44th AIAA Aerospace Sciences Meeting and Exhibit, Reno, Nevada, United States*, January 2006.

[5] Mukhopadhyay, V., Sobieszczanski-Sobieski, J., Kosaka, I., Quinn, G., and Charpentier, C., \Analysis Design and Optimization of Non-Cylindrical Fuselage for Blended-Wing-Body (BWB) Vehicle," *9th AIAA/ISSMO Symposium on Multidisciplinary Analysis and Optimization, Atlanta, Georgia, United States*, September 2002.

[6] Kroo, I., \Innovations in Aeronautics," *42nd AIAA Aerospace Sciences Meeting, January 5-8, 2004, Reno, NV*, 2004.

[7] Liebeck, R. H., Page, M. A., and Rawdon, B. K., \Blended-Wing-Body Subsonic Commercial Transport," *36th Aerospace Sciences Meeting and Exhibit, Reno, Nevada, United States*, January 1998.

[8] Roman, D., Allen, J. B., and Liebeck, R. H., \Aerodynamic Design Blended-Wing-Body Subsonic Commercial Transport," *18th AIAA Applied Aerodynamics Conference, Denver, Colorado, United States*, August 2000.

[9] Liebeck, R. H., \Blended Wing Body Design Challenges," *AIAA 2003-2659*.

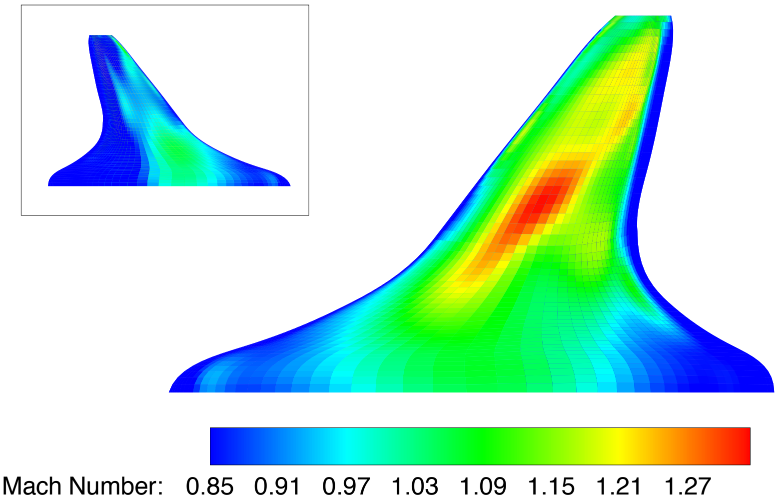


**Figure 15. Mach number distribution over the top and bottom (inset) surfaces of the section optimized BWB geometry.**

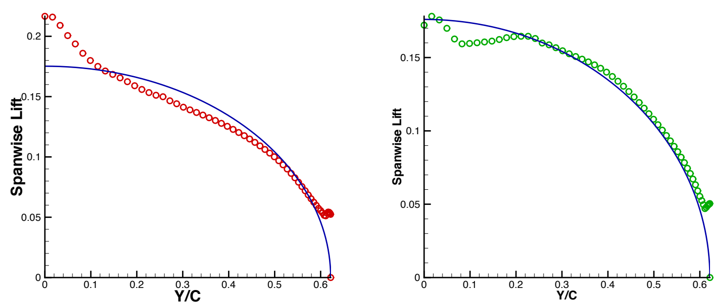


(a) Baseline geometry (b) Section optimized geometry

**Figure 16. Spanwise load distributions**


[10] Qin, N., Vavalle, A., and LeMoigne, A., \Spanwise Lift Distribution for Blended Wing Body Aircraft," *Journal of Aircraft*, Vol. 42(2), 2005, pp. 356{365.

[11] Siouris, S. and Qin, N., \Study of the EÞects of Wing Sweep on the Aerodynamic Performance of a Blended Wing Body Aircraft," *Journal of Aerospace Engineering*, Vol. 221(1), 2007, pp. 47{55.

[12] Pambagjo, T. E., Nakahashi, K., Obayashi, S., and Matsushima, K., \An Alternate Conþguration for a Regional Transport Airplane," *Transactions of the Japan Society for Aeronautical and Space Sciences*, Vol. 45(148), 2002, pp. 94{101.

[13] Pambagjo, T. E., Nakahashi, K., Obayashi, S., and Matsushima, K., \Aerodynamic Design Of A Medium Size Blended-Wing-Body Airplane," *39th AIAA Aerospace Sciences Meeting and Exhibit, Reno, Nevada, United States*, January 2001.

[14] Peigin, S. and Epstein, B., \Computational Fluid Dynamics Driven Optimization of Blended Wing Body Aircraft," *AIAA Journal*, Vol. 44(11), November 2006, pp. 2736{2745.

[15] Guynn, M. D., Freeh, J. E., and Olson, E. D., \Evaluation of a Hydrogen Fuel Cell Powered Blended-Wing-Body Aircraft Concept for Reduced Noise and Emissions," Tech. rep., NASA/TM-2004-212989, February 2004.

[16] Mart nez-Val, R., Perez, E., Alfaro, P., and Perez, J., \Conceptual Design of a Medium Size Flying Wing," *Journal of Aerospace Engineering*, Vol. 221, 2007, pp. 57{66.

[17] Bradley, K. R., \A Sizing Methodology for the Conceptual Design of Blended-Wing-Body Transports," Tech. rep., NASA/CR-2004-213016, September 2004.

[18] Torenbeek, E., *Synthesis of Subsonic Airplane Design*, Delft University Press, 1982.

[19] Kroo, I., \Aircraft Design: Synthesis, and Analysis," June 2010.

[20] Roskam, D. J., *Airplane Design - Part V: Component Weight Estimation*, Roskam Aviation and Engineering Corporation, 1989.

[21] Hicken, J. E. and Zingg, D. W., \Aerodynamic Optimization Algorithm with Integrated Geometry Parameterization and Mesh Movement," *AIAA Journal*, Vol. 48(2), 2010, pp. 400{413.

[22] Hicken, J. E. and Zingg, D. W., \A Parallel Newton-Krylov Solver for the Euler Equations Discretized Using Simultaneous Approximation Terms," *AIAA Journal*, Vol. 46(11), 2008, pp. 2773{2786.

[23] Giles, M. B. and Pierce, N. A., \An Introduction to the Adjoint Approach to Design," *Flow, Turbulence and Combustion*, Vol. 65, 2000, pp. 393{415.

[24] Gill, P. E., Murray, W., and Saunders, M. A., \SNOPT: An SQP Algorithm for Large-Scale Constrained Optimization," *SIAM Journal on Optimization*, Vol. 12(4), 2002, pp. 979{1006.

[25] UIUC Applied Aerodynamics Group, \UIUC Airfoil Coordinates Database," 2010.